Zoomorphology
DOI 10.1007/s00435-016-0339-2

ORIGINAL PAPER

The ultrastructure of escape organs: setose arms and cross-striated muscles in *Hexarthra mira* (Rotifera: Gnesiotrocha: Flosculariaceae)

Rick Hochberg[1] · **Hui Yang**[1] · **Jeffrey Moore**[1]

Received: 19 July 2016 / Revised: 29 November 2016 / Accepted: 9 December 2016

Abstract Rotifers are common prey of predatory zooplankton and have evolved a suite of defensive and escape strategies to avoid being consumed. Species of the genus *Hexarthra* are extraordinary in bearing six highly setose, arm-like appendages that function in saltational jumps through the water column to escape predation. To date, there are no observations on the structure of these escape organs despite their exceptionality within Rotifera. Here, we apply transmission electron microscopy (TEM) to study the ultrastructure of the arm-like appendages, their setae, and their muscle supply. TEM reveals that the arms are hollow extensions of the trunk integument with a similar ultrastructure. The integument is entirely syncytial. The syncytium is bordered apically by a double-layered plasma membrane beneath which is a layered cytoplasm: The top layer is a thin and fibrous intracytoplasmic lamina and the bottom layer is an electron lucent region containing cellular organelles bounded by a basal plasma membrane and thin basal lamina. Arm spines are hollow evaginations of the integument with no special ultrastructure. The arms terminate in primary setae that give rise to secondary setae, all of which possess an ultrastructure similar to the arms. There are two types of primary setae: unarticulated setae that are direct extensions of the arm integument, and articulated setae that fit into a ball-and-socket-type joint in the arm. Neither type is innervated nor supplied with muscles. The skeletal muscles in the trunk and arms are all cross-striated with distinct sarcomeres. All muscles are richly supplied with glycogen granules and mitochondria. A complex sarcotubular system supplies the myofibrils and is proximal to dense regions of glycogen, suggesting a glycolytic pathway for fast ATP production and the rapid release and reuptake of Ca^{2+} for muscle contraction.

Keywords Reynolds numbers · Zooplankton · Defense · Electron microscopy · Muscle ultrastructure

Introduction

Animals that live at low Reynolds numbers are said to inhabit a world of high viscosity, where inertial forces are negligible and powered locomotion depends on drag-based propulsion (Vogel 1996). Planktonic rotifers are microscopic invertebrates (0.1–2 mm) that live at very low Reynolds numbers, generally between 0.023 and 0.301 for animals 133–671 µm long that travel up to 2.849 mm/s (Santos-Medrano et al. 2001). And while swimming speed in rotifers is dictated largely by the abundance and distribution of their coronal cilia, other factors such as body shape also likely affect speed, as does the presence of any appendages that might supplement locomotion. For example, species of *Polyarthra* glide through the water at 0.348 mm/s (2.64 body lengths/s) using their corona, but can accelerate to more than 100 times gliding velocity (ca. 35.7 mm/s or 270 body lengths/s) when powering their 12 paddle-like appendages (Gilbert 1985, 1987; Kirk and Gilbert 1998). The paddles of *Polyarthra* are hollow extensions of the body wall and the cross-striated skeletal muscles that produce their movements insert on the integument around the paddles instead of inside them (Allen 1968). Contractions of these indirect muscles flex the body wall to create power and recovery strokes (Hochberg and Ablak Gurbuz 2008).

✉ Rick Hochberg
rick_hochberg@uml.edu

[1] University of Massachusetts Lowell, One University Avenue, Lowell, MA 01854, USA

Published online: 30 December 2016

Rotifer skeletal muscles are generally described as mono- or occasionally bicellular organs that may be cross-striated, oblique-striated, or smooth, engage in phasic or tonic contractions, and with high endurance (high volume of mitochondria/myoplasm) or not (Clément 1987; Clément and Amsellem 1989 and references therein). The cross-striated pattern is functionally linked with rapid movement of body parts as demonstrated for *Trichocerca rattus*, which has three pairs of cross-striated coronal retractors that withdraw the head for quick protection (Clément and Amsellem 1989). *Polyarthra vulgaris* also has cross-striated muscles that supply the corona as it does the paddles; the paddle muscles are also richly supplied with large mitochondria relative to the coronal retractors, implying their function in high endurance contractions (Allen 1968). These observations, along with a series of cytological measurements on a variety of other planktonic rotifers, led Clément and Amsellem (1989) to propose that the ultrastructure of rotifer skeletal muscles is more complex than striation patterns alone might suggest, and that observations of "jumping" rotifers such as species of *Polyarthra* might reveal additional details that are currently lacking about the structural and functional diversity of muscles in rapidly moving plankton.

In this study, we examine a species of jumping rotifer, *Hexarthra mira* (Hudson, 1871), using transmission electron microscopy. Species of *Hexarthra* (13 described species with numerous subspecies; Segers 2009) are exceptional because they possess six radially distributed appendages, each with their own direct muscle supply, and all bearing elongate setae that presumably function in drag-based locomotion (Hochberg and Ablak Gurbuz 2008). To date, there are no ultrastructural observations of any species of *Hexarthra*, and while it is known that they do possess cross-striated muscles—the striations can be observed with bright field microscopy—there are no cytological details about the individual muscles, their connections to the body wall, nor of the body wall itself, especially of the appendages. Our objectives are threefold: (1) to determine if the skeletal muscles of *H. mira* are similar to those of species from other genera that engage in rapid locomotion [e.g., species of *Polyarthra* (Ploima)]; (2) to examine the integument of the arms to determine if it differs from the trunk in a way that might have functional (locomotory) significance; and 3) to observe the fine structure of the setae to determine if their morphology provides any clues to their function, e.g., drag-based propulsion or sensation (Koehl 2001 and references therein).

Materials and methods

Specimens of *H. mira* were collected from Aeyers pond (Hudson, NH; 42°42′ 29.70″N, 71°25′10.41″W) with a 60-µm mesh plankton net in June 2016. Rotifers were photographed alive with a Zeiss A1 compound microscope equipped with DIC and a Sony Handicam digital camera. Six specimens were relaxed in 0.5% bupivacaine prior to fixation. One of the specimens was fixed in 4% paraformaldehyde in 0.05 M phosphate buffer (PB, pH 7.3) for 1 h prior to a rinse in PB with 0.5% Triton X-100 (30 min) and staining with Alexa Fluor-488 phalloidin (Life Technologies) for 1 h. The single specimen was mounted in Gel Mount (Electron Microscopy Sciences) and kept at −20 °C for 24 h. The slide was viewed on an Olympus FV 300 confocal laser scanning microscope equipped with argon laser. Fluoview software (Olympus) was used to collect a stack of 0.05-µm sections through an entire specimen mounted on its side. A single multi-TIF file was opened in Volocity software (PerkinElmer) to generate a z-stack and observe muscle orientations. Three of the six specimens were fixed in 2.5% glutaraldehyde in 0.1 M sodium cacodylate buffer (SCB; pH 7.3) for 2 h at room temperature. These specimens were then rinsed four times in 0.1 M SCB (15 min each), postfixed in 1% OsO_4 in 0.1 M SCB for 1 h, and rinsed again in SCB (4 × 15 min). The remaining two specimens were fixed directly in 1% OsO_4 for 1 h prior to a rinse in SCB as above. All fixed specimens ($n = 5$) were then dehydrated in an ethanol series (70, 90, 100, 100% × 10 min) followed by two rinses in propylene oxide (15 min each) and transitioned through a propylene oxide/Epon resin mixture (Araldite, EMbed 812; Electron Microscopy Sciences) series of 2:1 (1 h), 1:1 (1 h), and 1:2 (1 h), followed by an overnight embedding in pure Epon in a microcentrifuge tube on a rotator at room temperature. Specimens were cured in BEEM capsules in a 60 °C oven for 24 h. Epon blocks were trimmed and sectioned on a Reichert ultramicrotome, and sections were collected on Cu grids. Sections were stained with uranyl acetate (2 min) and lead citrate (2 min) and examined at 80 kV on a Philips CM10 equipped with Gatan Orius 813 digital camera at the Core Electron Microscope Facility at the University of

◀**Fig. 1** *Hexarthra mira*. **a** DIC photograph of live female specimen, lateral view. **b** TEM section through an adult female showing the large germovitellarium. **c** Ultrastructure of the dorsal integument close to the corona. Note the presence of the two layers. **d** Close-up of the apical plasma membrane showing two plasma membranes. **e** Ultrastructure of the trunk revealing small secretions outside of the integument. **f** Ultrastructure of the lateral body wall of the trunk showing vesicles in the integument and body cavity, small secretion drops outside the integument, and a vesicle apparently in the process of secretion (*). *1* Top layer of the syncytial cytoplasm (intracytoplasmic lamina) of the integument, *2* bottom layer of the syncytial cytoplasm of the integument, *ap* apical plasma membrane(s), *bc* body cavity, *bl* basal lamina, *bp* basal plasma membrane, *cr* corona, *da* dorsal arm, *dt* dorsal antenna, *gc* glycocalyx, *gl* glycogen, *gv* germovitellarium, *la* lateral arm, *mi* mitochondria, *mu* muscle, *nu* nucleus, *sd* small secretion drops, *st* setae, *ve* vesicle. *Scale bars* **a** 40 µm, **b** 15 µm, **c** 500 nm, **d** 100 nm, **e** 200 nm, **f** 900 nm

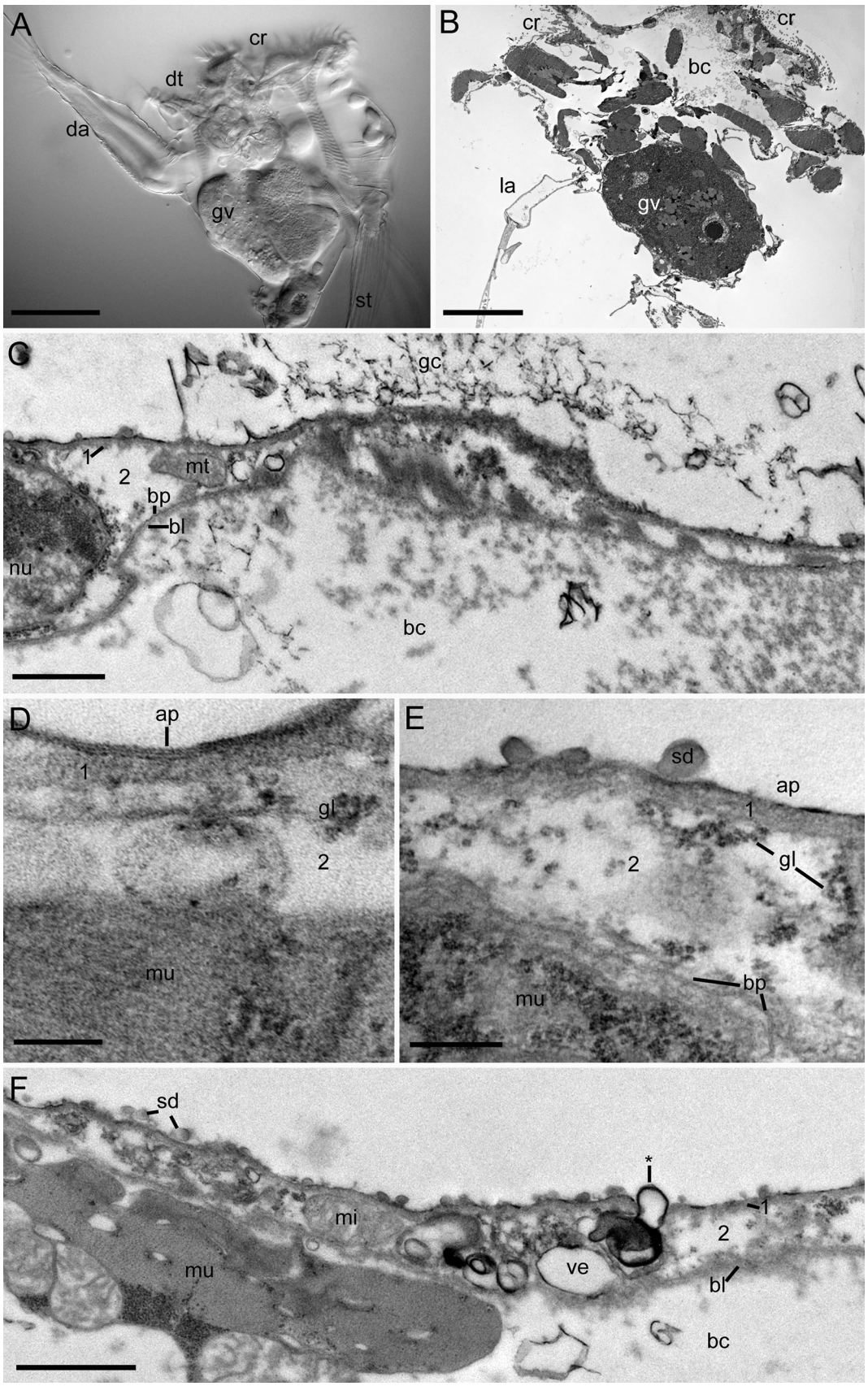
A
cr
dt
da
gv
st
B
cr
cr
bc
la
gv
C
gc
1
2
mt
bp
bl
nu
bc
D
ap
1
gl
2
mu
E
sd
ap
1
2
gl
mu
bp
F
sd
*
mi
1
2
mu
ve
bl
bc

Massachusetts Medical School in Worcester, MA. Digital images were not manipulated except for basic cropping and some changes in brightness and contrast using Adobe Photoshop CS 5. Measurements of cells and organs were taken with ImageJ 1.45 s.

Results

Trunk Integument The integument of the trunk is relatively smooth and homogeneous in appearance when viewed with DIC and transmission electron microscopy (Fig. 1). There were some notable and very small spine-like protrusions detectable at the ultrastructural level, but these were not consistent across the integument (not shown). The integument rarely had any distinguishable glycocalyx, though when present, it was fibrous in appearance (Fig. 1c). Small secretion-like drops (50–120 nm in diameter) were occasionally present outside the integument (Fig. 1e, f). The syncytial integument consisted of one or more apical plasma membranes over a thin cytoplasm consisting of two layers: The most apical layer (layer 1) was the intracytoplasmic lamina (ICL) and layer 2 was the electron lucent cytoplasm containing organelles (Fig. 1c–f). The basal plasma membrane was bordered by a thin basal lamina separating it from the body cavity. The entire integument measured up to 1.72 μm thick, but this was only in regions that contained a nucleus (e.g., 2.5 μm long × 1.46 μm high; Fig. 1c). Most of the integument was less than 450 nm thick, with most regions ($n = 65$ sections across five specimens) measuring less than 380 nm thick across the trunk.

The plasma membranes of the integument were not distinct in all specimens or in all regions of the body, but in general appeared to have a trilaminar (electron dark–light–dark) appearance that measured ca. 4–6 nm thick. In several regions, we noted that there appeared to be two plasma membranes as evidenced by dark–light–dark–light–dark bands (Fig. 1d) that measured up to 13 nm in thickness. Immediately beneath the plasma membrane(s) was the ICL (layer 1), which was consistently electron dense in all specimens. It had a mostly fibrous appearance and never showed evidence of any contained organelles or any changes in electron density across the body (Fig. 1d, e). The ICL measured 60–80 nm thick in all sections of the trunk.

Layer 2 consisted of electron lucent cytoplasm where all cellular organelles and secretions were present including nuclei, mitochondria, a variety of membrane-bound vesicles, and glycogen granules (Fig. 1c–f). Layer 2 measured up to 407 nm thick where vesicles and mitochondria were present, but in many sections, layer 2 appeared nearly absent, showing only a very thin electron lucent region between the ICL and basal plasma membrane (not shown). Mitochondria often appeared squeezed with no space between ICL and the basal plasma membrane; they measured 300–390 nm maximum in cross section. No vase-shaped vesicles (i.e., hypodermal bulbs *sensu* Storch and Welsch 1969; Schramm 1978; Clément and Wurdak 1991) were observed, but several membrane-bound vesicles of oblong and irregular shapes were present (Fig. 1f). The vesicles always had an electron dense membrane and measured 70–300 nm long. Most integumentary vesicles had electron lucent cores, but some contained electron dense materials that in some cases appeared to be in the process of being released from the integument (Fig. 1f). These vesicles were not similar to the vesicle-like structures observed in the body cavity, which were often much larger (up to 900 nm diameter; Fig. 1c, f) and irregular in shape (Fig. 2d). Beneath layer 2 was the basal plasma membrane, which was trilaminar in appearance and 4–6 nm thick. It was always bordered by a basal lamina up to 30 nm thick.

Arm integument The integument of the arms was mostly smooth, but did show evidence of a wavy outline with DIC microscopy, particularly toward the proximal end of the arm nearest the shoulder (Fig. 2a). TEM also revealed this wavy outline (Fig. 2b, c), but not in all sections nor in all arms (Fig. 2d), which might be the result of the plane of section. The fine structure of the arms was similar to the trunk with an identical layering of plasma membrane (always double-layered), thin ICL, thin or nearly absent electron lucent cytoplasm (see Fig. 3b), basal plasma membrane, and thin basal lamina (Figs. 2, 3). There were no obvious differences in ultrastructure between the proximal and distal regions of the arms. The integument was always relatively thin and never measured more than 330 nm thick, with maximum thicknesses of 160 nm for the ICL (layer 1) and 170 nm for layer 2. The arm ICL had a similar fibrous appearance to the trunk ICL, although in some sections it appeared somewhat granular. The clear cytoplasm of layer 2 had few organelles other than mitochondria and rarely vesicles, and in some regions of the arms the cytoplasm was so thin (<4 nm thick) that it was nearly absent (Fig. 3b). The integument of the arm spines was identical in structure and thickness to the rest of the arm (Fig. 3a, b).

Arm setae Only the setae of the dorsal and ventral arms were observed due to the orientations of the specimens. Setae were arranged as primary setae that project from the distal end of the arms and secondary setae that project from the primary setae (Fig. 3c). There are several secondary setae per primary seta. All setae are syncytial and consist of an apical plasma membrane atop an ICL (layer 1) that surrounds an electron lucent cytoplasm (layer 2) (Fig. 3d,

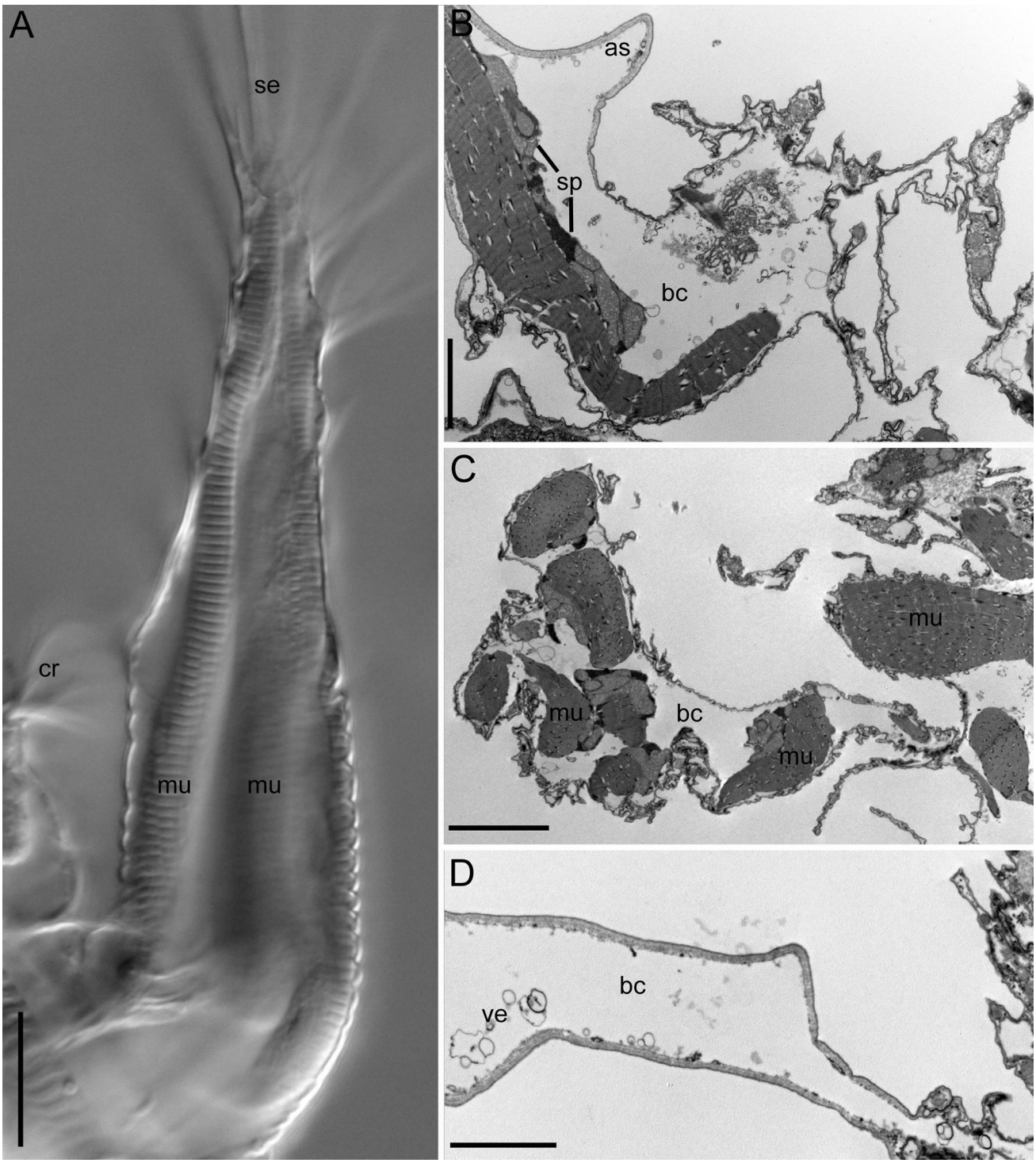

Fig. 2 Arms of *H. mira*. **a** DIC photograph of lateral arm revealing the striated muscles and setae. **b** TEM section through the dorsal arm around the shoulder junction; distal is to the left. **c** TEM section (oblique) through a lateral arm. **d** TEM section (tangential) through a lateral arm showing its hollow structure (section missed all skeletal muscles). *as* arm spine, *bc* body cavity, *cr* corona, *mu* skeletal muscle, *sp* sarcoplasm with mitochondria and glycogen granules, *ve* vesicles in the body cavity. *Scale bars* **a** 19 µm **b** 2.5 µm, **c** 4 µm, **d** 3 µm

e). Tangential sections through the ICL always showed it to be highly fibrous (Fig. 3f). There appeared to be two different kinds of primary setae based on their connections with the arms: unarticulated setae (Fig. 3a) and articulated setae (Fig. 4b). These setae could not be distinguished with DIC microscopy. Both setae are similar in ultrastructure except for their connections to the arms. The unarticulated setae are direct extensions of the arm integument and share

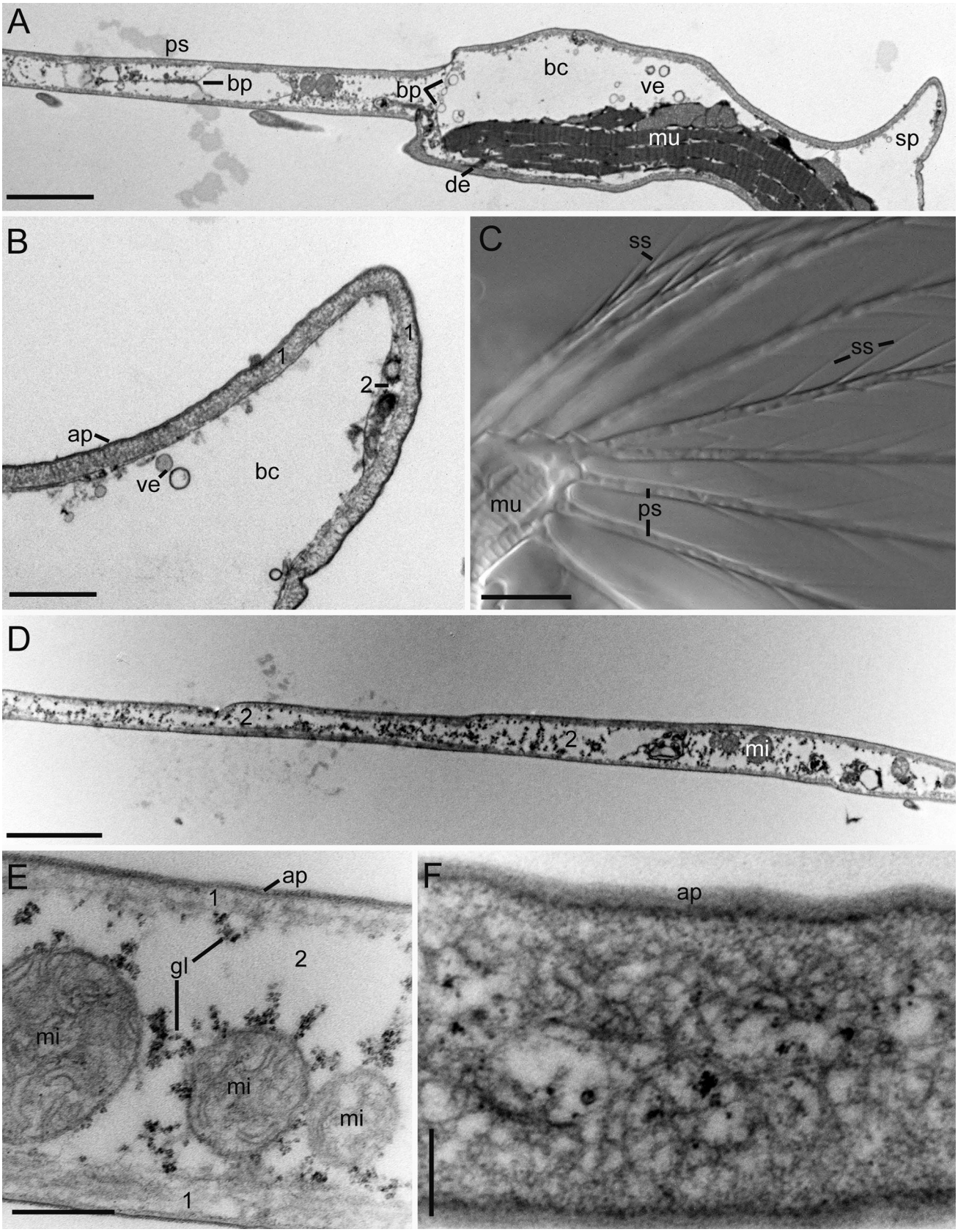
A
ps
bp
bp
bc
ve
mu
sp
de
B
1
1
2
ap
ve
bc
C
ss
ss
mu
ps
D
2
2
mi
E
ap
1
gl
2
mi
mi
mi
1
F
ap

◀**Fig. 3** Fine structure of arms and setae in *H. mira*. **a** TEM longitudinal section through the distal end of the dorsal arm. The skeletal muscle inserts on the basal plasma membrane of the integument. The section shows only a single primary seta. **b** Ultrastructure of an arm spine. Note the integument has a thick ICL (layer 1) but thin layer 2. **c** DIC photograph of the setae on a lateral arm showing both primary and secondary setae. **d** TEM section through an unarticulated primary seta. **e** Ultrastructure of a primary seta revealing that the seta is not hollow but is instead an extension of the syncytial arm integument. *1* Top layer (intracytoplasmic lamina) of the syncytial integument, *2* bottom layer (electron lucent cytoplasm) of the syncytial integument, *ap* apical plasma membrane, *bc* body cavity, *bp* basal plasma membrane of the integument, *de* desmosome, *mi* mitochondria, *mu* skeletal muscle, *ps* primary setae, *sp* arm spine, *ss* secondary seta, *ve* vesicle. *Scale bars* **a** 2 μm, **b** 600 nm, **c** 4 μm, **d** 500 nm, **e** 350 nm, **f** 300 nm

a common ultrastructure (apical plasma membrane, ICL, and basal cytoplasm) (Fig. 3a). The body of each seta is essentially a narrow continuation of the arm and consists almost entirely of cytoplasm and abundant mitochondria, glycogen, and vesicles (Figs. 3a, d, e, 4a). Mitochondria had a larger cross-sectional diameter (to 600 nm) than present in the body integument. Some longitudinal sections revealed a thin plasma membrane dividing the seta down its long axis, suggesting that the seta is not merely an extension of a continuous cytoplasm but that it is a fold in the integument, i.e., the dividing membrane is actually two adjacent basal plasma membranes that come together (Figs. 3a, 4a). The second type of primary setae is an articulated seta that fits into a socket-like connection on the arm (Fig. 4b). These setae protruded from a small indentation at the distal end of the arm. In longitudinal section, there was very little continuity between the arm integument and the seta integument. In fact, the apical membrane of the seta appeared to encase the base where it formed the socket joint (Fig. 4b), although there might be small areas of cytoplasmic continuity between arm and seta (Fig. 4b). Most socket joints were more electron dense than the surrounding integument of the arm and setae. The joints had several small membrane-bound vesicles in the socket between arm and primary seta (Fig. 4b). Unfortunately, none of our sections revealed a clear view of the connection between primary and secondary seta, so we are uncertain if secondary setae are unarticulated or articulated. Still, all secondary setae do appear to be syncytial and of similar ultrastructure to the primary seta (Fig. 4d).

Muscles

Our observations are based on relaxed specimens only. We used CLSM observations (Fig. 5a) to correlate gross morphology and positions of muscles with observations at the ultrastructural level. The muscle patterns of *H. mira* have already been described (see Šanto et al. 2005; Hochberg and Ablak Gurbuz 2008). We note that all skeletal (somatic) muscles appeared cross-striated with both CLSM and TEM (Figs. 2a–c, 3a, 5). The muscles that supplied the arms originated in the body and took circuitous routes toward their insertions (Fig. 5a); hence, ultrathin sections never revealed an entire muscle along its length, and so their origins were difficult to identify with certainty.

Muscles were generally strap-shaped, and their transverse profiles ranged from somewhat compressed (Fig. 5b) to circular and oblong (Fig. 5c). The basal lamina was either extremely thin or apparently absent around individual muscles; specimens fixed alone in OsO_4 or double-fixed in GA followed by OsO_4 yielded identical results regarding the near absence of basal lamina, so this does not appear to be a fixation artifact (also, basal lamina was always present beneath the integument). Each muscle consisted of a single myofibril contained within a tightly appressed sarcolemma. The subsarcolemmar cytoplasm (sarcoplasm) was electron dense and highly granular with abundant glycogen granules and contained numerous large mitochondria (up to 550 nm in cross section; up to 2 μm long). A single nucleus was observed in most muscles (ca. 1.4 μm in cross section), but most muscles were not serially sectioned, so additional nuclei could be present. The nuclei were electron dense, had several darker nucleoli (Fig. 5b), and differed in appearance from the nuclei of the body wall (Fig. 1). Several sections revealed organelles between the myofibrils (Fig. 5c), but these are interpreted as oblique sections, where the sarcoplasm and the underlying myofilaments were caught at different angles along the length of a muscle fiber because of the muscle's wavy outline. In other sections, several oblique (almost cross-sectional) profiles of a single muscle fiber were obtained, with two or more regions of myofilaments connected by elongate regions of sarcoplasm containing abundant mitochondria (Fig. 5d). Some mitochondria were surrounded by multiple membranes (Fig. 6a, d) reminiscent of membraneous extensions of the endoplasmic reticulum known as whorl bodies present in some vertebrate neurons (e.g., Fernández et al. 1986) and the muscles of teleost fish (e.g., Brantley et al. 1993; Kéver et al. 2014). Most muscles had a sarcolemma that was tightly appressed to the myofilaments beneath, with almost no granular cytoplasm in between (Fig. 5c, d).

The myofilaments formed well-defined sarcomeres with recognizable A bands, I bands, H-zones and straight (continuous) Z-lines. Several cross sections revealed profiles of M-lines and/or H-zones, i.e., there were no thin filaments present around the thick filaments (Fig. 6c). Thick filaments formed hexagonal patterns (Fig. 6c), and most filaments were ca. 12–13 nm in diameter with a consistent lattice spacing of 19 nm, which is closer than that found in vertebrate striated muscles ($\sim$35 nm; Irving

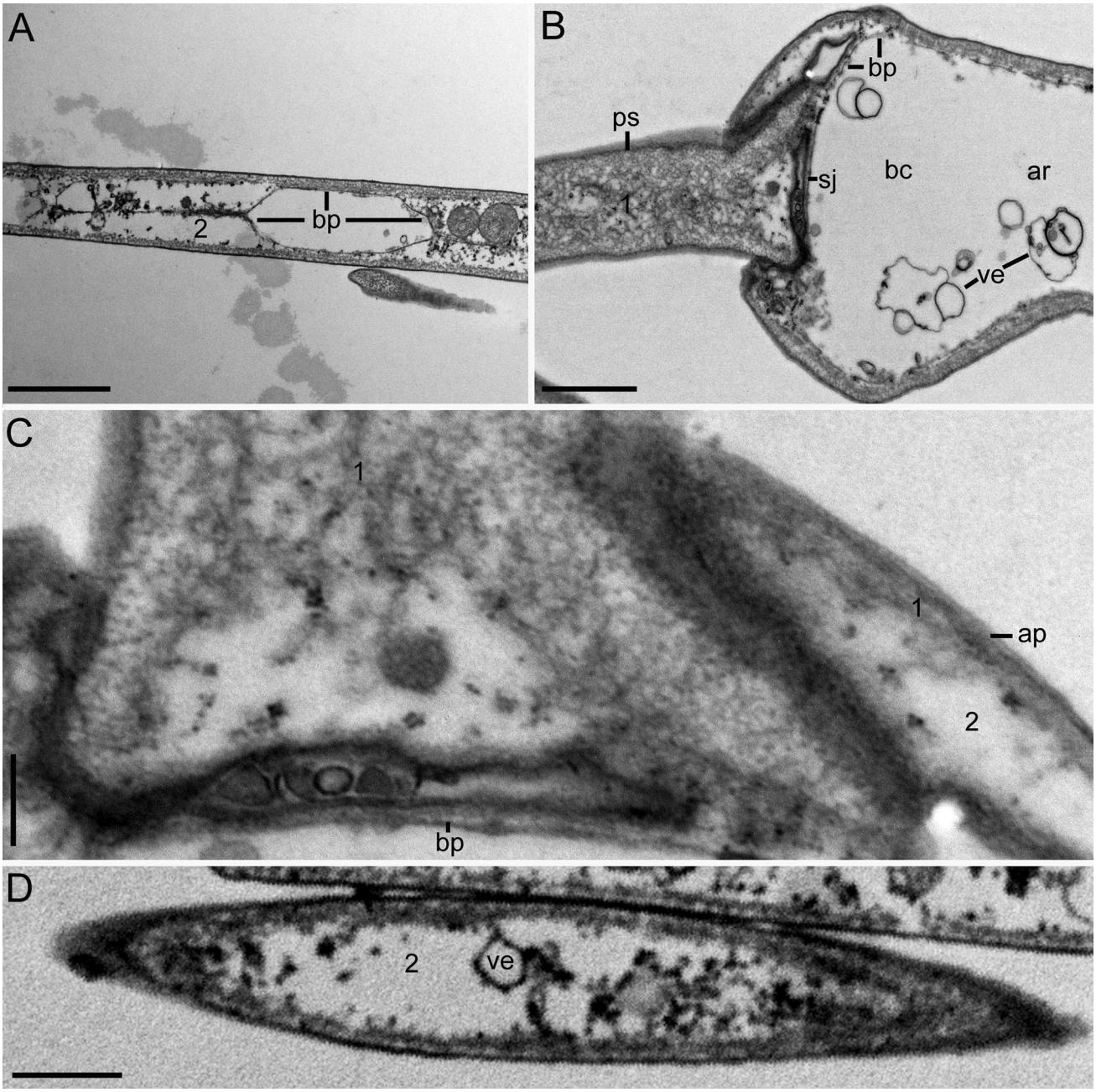

Fig. 4 Fine structure of primary and secondary setae in *H. mira*. **a** Close-up of primary seta (see Fig. 3a for wider view). Note the hollow gap in the seta where there are two basal plasma membranes, interpreted here as a fold in the integument to produce the seta. **b** Close-up of the joint of a primary articulated setae. The primary seta appears to fit into a small joint at the terminus of the arm. **c** Closer view of the joint in B. **d** Tangential section through a secondary seta next to a primary seta (above). *1* Top layer (intracytoplasmic lamina) of the syncytial integument, *2* bottom layer (electron lucent cytoplasm) of the syncytial integument, *ap* apical plasma membrane, *ar* arm terminus, *bc* body cavity, *bp* basal plasma membrane(s), *sj* seta joint, *ve* vesicles. *Scale bars* **a** 1.2 µm, **b** 1 µm, **c** 150 nm, **d** 300 nm

et al. 2011). Small protrusions from the thick filaments could be seen in some micrographs, which may indicate M-bridges (Fig. 6e). Thick filaments had a solid core in the region of M-lines and H-zones, but appeared hollow outside of these regions similar to the hollow thick filaments observed with arthropod muscles (e.g., Reedy 1968; Levine et al. 1983) (Fig. 6e). Our micrographs did not permit accurate counts of thin filaments. Z-material was 22–26 nm wide in longitudinal sections. Sarcomere lengths in the skeletal muscles of the main body were 1.087–1.351 µm long ($n = 50$ from five muscles from three specimens; mean = 1.188 µm), while those of the coronal retractors were

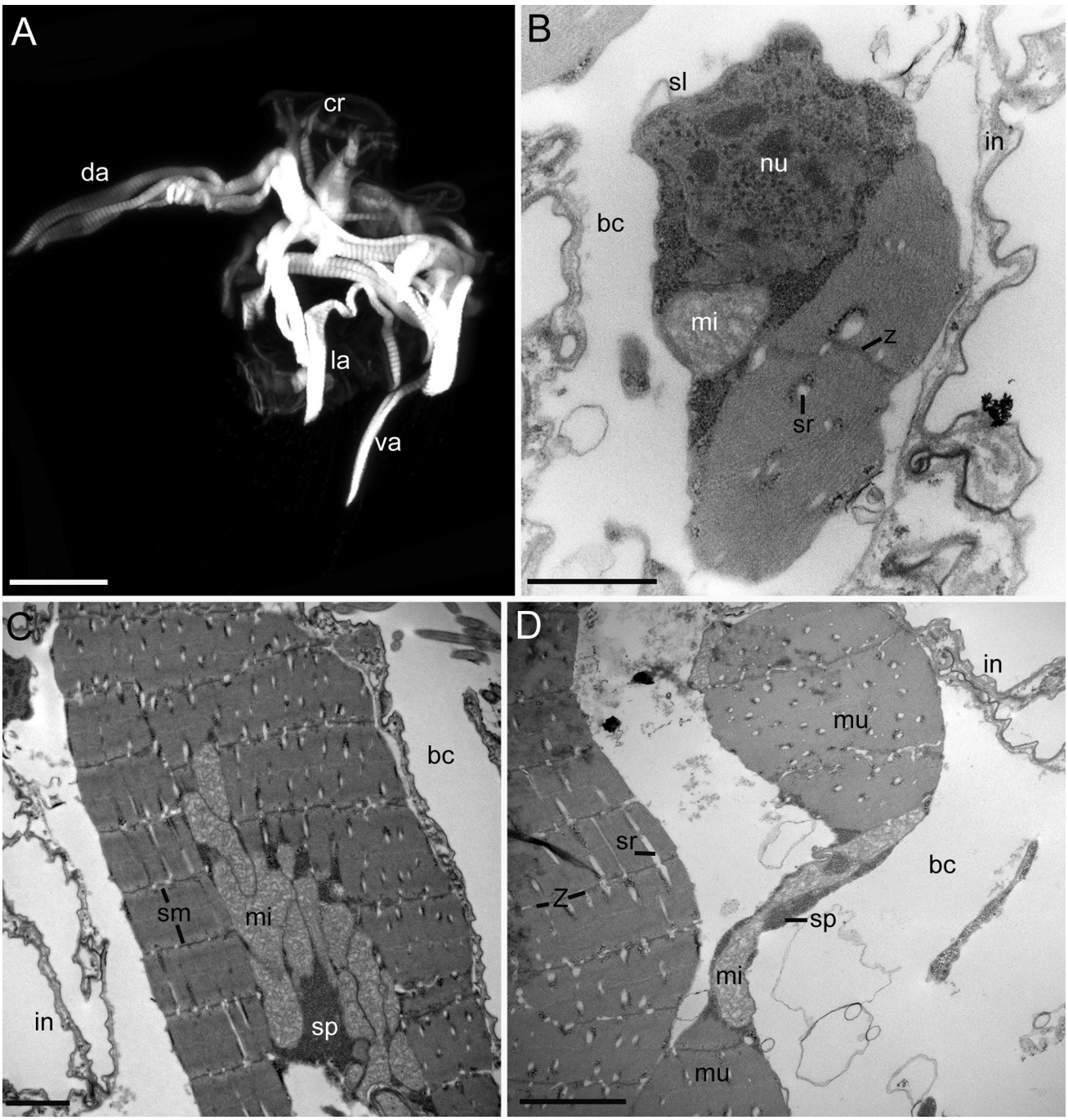

Fig. 5 The musculature of *H. mira*. **a** CLSM z-stack of a specimen in lateral view showing the undulating skeletal (somatic) muscles of the trunk and arms. Z-lines are evident in the photograph. **b** Slightly oblique section through a single trunk myofiber bound by a tight sarcolemma and including a nucleus and mitochondrion to one side of the myofibrils. **c** Slightly oblique longitudinal section through a skeletal muscle revealing numerous sarcomeres. The central sarcoplasm with mitochondria is an artifact of the section plane (see text for details). **d** Section through two trunk muscles, one longitudinally (*left*) and one that is heavily curved (*right*). The curved muscle shows two oblique profiles through the myofibrillar portion and a central sarcoplasmic connection between them (see text for details). *bc* body cavity, *cr* coronal retractors, *da* dorsal arm, *in* integument of the body wall, *la* lateral arm, *mi* mitochondria, *mu* skeletal muscle, *nu* nucleus, *sl* sarcolemma, *sm* sarcomere, *sp* sarcoplasm, *sr* sarcoplasmic reticulum, *va* ventral arm, *Z* Z-line. *Scale bars* **a** 50 μm, **b** 600 nm, **c** 1 μm, **d** 1 μm

921 nm – 1.027 μm long. Most arm muscles were not sectioned longitudinally due to the arms' orientations, making sarcomere length determination difficult. However, we did obtain a mostly longitudinal profile through the dorsal arm, which had an average sarcomere length of 741.1 ± 39.8 nm (n = 33 sarcomeres; range 712–833 nm).

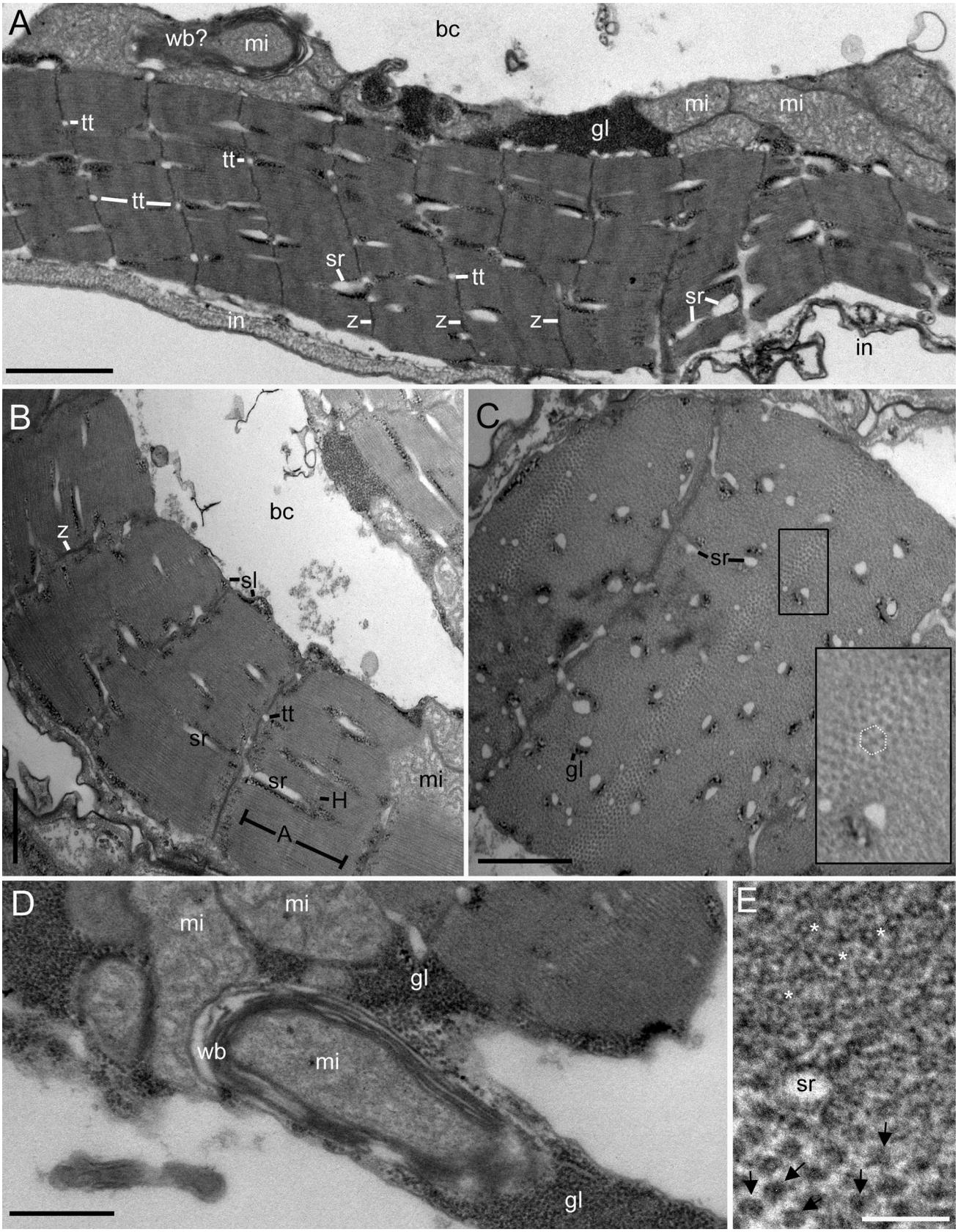
A
wb?
mi
bc
mi
mi
gl
tt
tt
tt
sr
tt
sr
in
z
z
z
in
B
bc
z
sl
tt
sr
sr
mi
H
A
C
sr
gl
D
mi
mi
gl
wb
mi
gl
E
*
*
*
*
sr

◀**Fig. 6** Ultrastructure of the muscles of the arms and trunk of *H. mira*. **a** Close-up of a skeletal muscle in the dorsal arm revealing abundant mitochondria in the peripheral sarcoplasm and the highly ordered nature of the cross-striated myofilaments. Note the abundant T-tubules and sarcoplasmic reticulum between the myofibrils. **b** Close-up of a longitudinal muscle in the trunk showing the structure of a sarcomere. **c** Oblique (almost cross) section a single myofiber with abundant sarcoplasmic reticulum. The *inset* shows a magnified region of an apparent H-zone, with thick filaments forming a hexagonal pattern. **d** A potential whorl body (lamellate sarcoplasmic reticulum; see, e.g., Brantley et al. 1993) surrounding a mitochondrion in the peripheral cytoplasm of a muscle fiber (see also **a** above). **e** Magnified view of the thick filaments inside and outside the H-zone. *Dark arrows* show electron dense thick filaments of the H-zone, and *asterisks* (*) reveal thick filaments with a hollow core outside the zone. *A* A band, *bc* body cavity, *gl* glycogen granules, *H* H-zone, *in* integument, *mi* mitochondria, *sl* sarcolemma, *sr* sarcoplasmic reticulum, *tt* T-tubule, *Z* Z-line, *wb* whorl body. *Scale bars* **a** 1 μm, **b** 700 nm, **c** 500 nm, **d** 500 nm, **e** 50 nm

Sarcomere lengths in two of the lateral arms (one right and left arm) measured 669–765 nm long (left arm: mean = 695.6 ± 19.85 nm; right arm: mean = 725 ± 20.02).

The sarcotubular system was highly complex and consisted of numerous branches of intramyrofibril sarcoplasmic reticulum (Figs. 4, 5, 6). The SR was abundant in longitudinal and oblique/cross-sectional profiles and protruded into the myofibrils. SR tubules were ca. 50–70 nm wide and often as long as a sarcomere in longitudinal section, while transverse sections of SR were 23–83 nm diameter. Glycogen granules were regularly present next to the SR in the myoplasm. T-tubules were located at Z-lines and had diameters of 53–90 nm (Fig. 6). Dyads were rarely observed, and triads were never observed.

All skeletal muscles inserted on the integument through multiple cell–cell adherens junctions, both within the main body (Fig. 7a, b) and along the length of the arms and at its terminus (Fig. 7c–e). Adherens junctions consisted of an electron dense plaque between the sarcolemma and the basal plasma membrane of the integument (Fig. 7e). Similar junctions were present between the coronal retractor muscles and the ciliary cushions of the corona (not shown).

Discussion

The three-dimensional environment of planktonic rotifers is one of perpetual exposures, where predators can attack from all flanks, and where rapid detection, escape, and deterrence are necessities for survival. Rotifers have evolved a variety of ways to avoid or escape immediate predation such as brief increases in swimming speed (Gilbert and Kirk 1988; Kirk and Gilbert 1998), chemical deterrence (Felix et al. 1995), camouflage (retracting into gelatinous sheaths, Williamson 1983), and spine protrusion (Wallace et al. 2015). An alternative strategy is evasive locomotion, which is generally found among rotifers that have accessory appendages. Species of *Filinia* (Gnesiotrocha: Filinidae) have three elongate setae (two of which are mobile) that are proposed to generate thrust and lead to evasion (Wallace et al. 2015; but see alternative explanations by Williamson 1987; Hochberg and Ablak Gurbuz 2007). Species of *Hexarthra* (Gnesiotrocha: Hexarthridae) have six setose-bearing arm-like appendages that function in rapid jumps through the water column (Kak and Rao 1998; Hochberg and Ablak Gurbuz 2008), and species of *Polyarthra* (Ploima: Synchaetidae) have 12 paddle-like appendages that likewise produce quick jumps (Allen 1968; Gilbert 1985, 1987; Kirk and Gilbert 1998; Hochberg and Ablak Gurbuz 2008). Other species with moveable appendages (e.g., species of the *Notholca striata* clade have moveable spines; Wallace and Colburn 1989) presumably use them as deterrents and not for mobility. Previous studies have revealed that the appendages of both *Filinia* and *Polyarthra* are hollow extensions of the trunk integument and that cross-striated muscles function in both power and recovery strokes to generate quick appendage movement (Allen 1968; Šanto et al. 2005; Hochberg and Ablak Gurbuz 2007, 2008). Here, we examined the appendages and muscles of *H. mira* to determine if there are any ultrastructural similarities among the escape organs (arms, muscles) of the three taxa that have been described with TEM, and to provide detailed insights into the muscles that power appendage movement.

The mobile arms of *Hexarthra*, like the setae of *Filinia* and the paddles of *Polyarthra*, are unique appendages within the Rotifera. All three are extensions of the trunk integument, which is always syncytial and consists of two layers: an apical intracytoplasmic lamina (layer 1) and a basal electron lucent cytoplasm (layer 2). These features are easily observed in *H. mira*, but in the latter two species, the photomicrographs and descriptions are inadequate to draw more detailed comparisons (Allen 1968; Hochberg and Ablak Gurbuz 2007). Still, it is evident that the arms of *H. mira* have a much thinner integument than exists in the setae of *Filinia* or the paddles of *Polyarthra*, where the ICL appears to be quite thick and rigid. The rigidity of these appendages be maintained by the hydrostatic pressure of the rotifers' body cavities, which are continuous with the appendages in all three taxa (Allen 1968; Hochberg and Ablak Gurbuz 2007, 2008). Appendage movements in species of *Filinia* and *Polyarthra* are powered through contraction of indirect skeletal muscles, i.e., the muscles originate in the trunk and insert around the shoulder of each appendage instead of inside them. The muscles are cross-striated, though few observations have been made about their ultrastructure (Allen 1968; Hochberg and Ablak Gurbuz 2007). In *H. mira*, the arms are also hollow, but the muscles supply the appendages directly, extending from

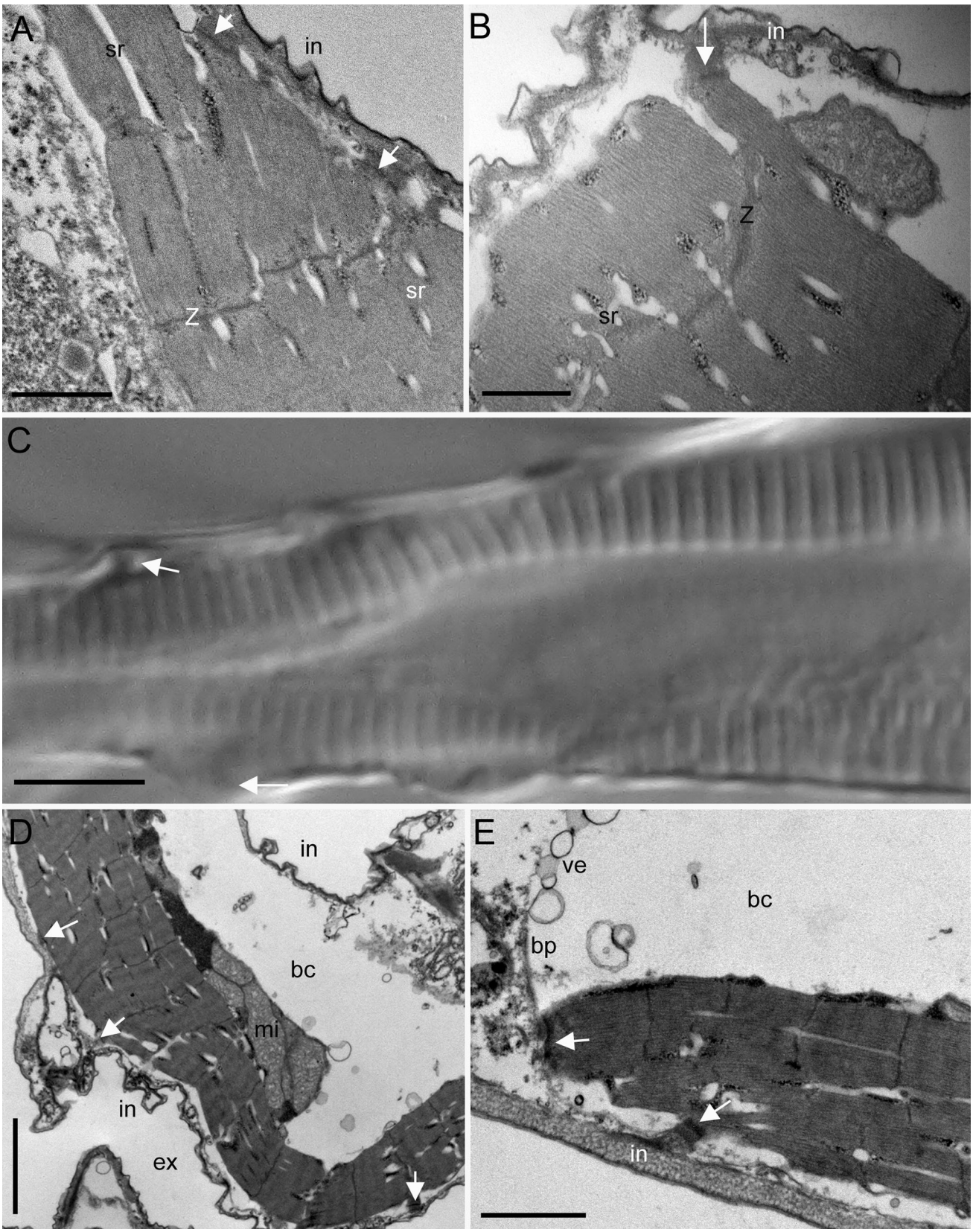
A
sr
in
Z
sr
B
in
Z
sr
C
D
in
bc
mi
in
ex
E
ve
bc
bp
in

◀**Fig. 7** Cell-to-cell adherens junctions (desmosomes) between a striated muscle and the integument in *H. mira*. **a** Desmosome (*arrows*) showing the origins of skeletal muscles in the trunk. **b** Desmosome between a skeletal muscle and the trunk integument. Layer 2 of the integument protrudes toward the muscle. **c** DIC micrograph of an arm showing potential sites of cell-to-cell connections (*arrows*) between muscles and the integument of the arm. **d** Longitudinal section through the shoulder region of an arm revealing multiple desmosomes. **e** Distal end of an arm displaying a skeletal muscle contacting the basal plasma membrane of the arm integument. *bc* body cavity, *bp* basal plasma membrane of the integument, *ex* external environment, *in* integument, *mi* mitochondria, *sr* sarcoplasmic reticulum, *ve* vesicles, *Z* Z-line. *Scale bars* **a** 1 μm, **b** 400 nm, **c** 10 μm, **d** 1.5 μm, **e** 700 nm

their origins in the trunk to their insertions inside the arms where they make multiple adherens junctions with the integument. Each arm is supplied with at least two separate muscles that probably function separately in power and recovery strokes (Hochberg and Ablak Gurbuz 2008).

The skeletal muscles of the trunk and arms share identical ultrastructures, with each muscle consisting of a single myofiber that may be branched or folded. The myofibers are surrounded by a tightly appressed sarcolemma (i.e., rarely undulating), and the subsarcolemmar cytoplasm contains an occasional nucleus, abundant glycogen, and numerous mitochondria. The cross-banded pattern of the myofibrils is apparent even with bright field microscopy, and with TEM shows intensely stained A bands (myosin) and less intensely stained I bands (mainly actin), characteristic of cross-striated muscles in rotifers (Amsellem and Clément 1977, 1988). Cross sections through the skeletal muscles reveal an apparent gradation in the thick myofilaments from a solid core in the M bands and/or H-zones to a hollow core outside these areas, which is indicative of the presence of paramyosin (Levine et al. 1983; Epstein et al. 1985). Clément and Amsellem (1989) noted only hollow cores in the thick filaments of skeletal muscles in *T. rattus*, the only other rotifer examined in comparable detail. The thick filaments of *H. mira* have a diameter of 12–13 nm, which is smaller than the thick filaments (15 nm) of *T. rattus* (Clément and Villeneve 1971; Amsellem and Clément 1977, 1988). These diameters are both at the lower end of the size spectrum for most invertebrates where the range is generally 18–30 nm, with some animals achieving much larger diameters (reviewed in Hooper et al. 2008). Unfortunately, our micrographs did not permit clear views of thin filaments, so we are uncertain about the thick/thin myofilament ratios. The Z-lines are straight, perpendicular to the long axis, and co-parallel along a fiber's length, and the Z-material is mostly continuous with occasional interruptions by sarcoplasmic reticulum and t-tubules. In *T. rattus*, the Z-material is somewhat discontinuous (described as reticulated by Amellem and Clement 1988) and consists of distinct dense bodies, especially at supercontraction. None of the muscles in *H. mira* appeared contracted, so we are uncertain if the Z-material becomes differently organized as it does in *T. rattus* during a contracted state.

Glycogen granules are present in the subsarcolemmal space around mitochondria, which is similar to other rotifers (see Amsellem and Clément 1977), but in *H. mira*, the granules are also dispersed heavily among the myofibrils, especially evident around the sarcoplasmic reticulum. This is similar to the condition in vertebrate cross-striated muscles, where ß-particles of glycogen are present between myofibrils and among filaments in individual myofibrils, generally in the I band (Vye 1976). The proximity of glycogen to SR within myofibrils is thought to function as a rapid source of glycolytic ATP to Ca^{2+}-ATPase pumps in the SR, which leads to faster Ca^{2+} transport and hence muscle contraction compared to oxidative phosphorylation (Xu et al. 1995; Xu and Becker 1998; reviewed in Rakus et al. 2015). Additionally, the SR within the skeletal muscles of *H. mira* is highly complex and consists of numerous invaginations that penetrate all muscles both transversely and longitudinally. The high amounts of SR, and their proximity to glycogen granules, would seem to indicate the potential for a rapid release and reuptake of Ca^{2+}. In fact, the proximity between SR invaginations and myofibrils narrows the diffusion distance for Ca^{2+} to only a few dozen or hundred nanometers, which would imply that the skeletal muscles of *H. mira* evolved for fast contraction–relaxation cycles. These data support the observations of the rotifer's behavior (Hochberg and Ablak Gurbuz 2008). Similar findings on the complexity of the SR in rotifers are noted for *T. rattus*, which has striated muscles that control the movement of its articulated tail (Clément and Amsellem 1989).

We speculate that muscle endurance and speed in rotifers are probably dictated by the same cellular and ultrastructural properties measured in other invertebrates (Royuela et al. 2000). In fact, the skeletal muscles of *H. mira* possess many of the same ultrastructural properties that characterize the "fast" muscle fibers of other animals (Royuela et al. 2000), particularly arthropods (Josephson and Young 1987; Josephson et al. 2000). For example, the abundance of mitochondria is known to affect muscle endurance, and here we find that all skeletal muscles of *H. mira* are richly supplied with subsarcolemmal mitochondria. However, without quantitative measurements, we are uncertain if the striated muscles of *H. mira* have a greater or lesser endurance than other invertebrates, particularly the rotifer *T. rattus*. In the latter species, the highest endurance among skeletal muscles was hypothesized for the lateral retractors, which have the maximum volume of mitochondria/cytoplasm (Clément and Amsellem 1989). However, this rotifer is not a quick moving species and

only relies on its lateral retractors for withdrawal, not escape. These retractor muscles therefore have a relatively slow speed of shortening (Clément and Amsellem 1989) and are not sufficient for comparison to the skeletal muscles of *H. mira*. Still, it would seem that endurance is less important than speed of contraction, particularly for rotifers that engage in short bouts of evasive locomotion.

Speed of contraction is dependent on the abundance and complexity of the sarcotubular system (sarcoplasmic reticulum and T-tubules), as well as the length of the sarcomeres (Clément and Amsellem 1989) and other factors (Rakus et al. 2015). In *H. mira*, the SR is highly complex, and along with its abundance and proximity to glycogen granules (noted above), would indicate the potential for high-speed contractions. T-tubules are also numerous, but perhaps surprisingly, there was little evidence of dyads and no evidence of triads (for excitation–contraction coupling), which would corroborate our speculations about "fast" muscles in this species. Another limitation here is that data on the SR of cross-striated muscles in rotifers, including variations in sarcomere length, are mostly limited to *T. rattus*, which does not engage in evasive behaviors (Clément and Villeneve 1971; Amsellem and Clément 1977, 1988; Clément and Amsellem 1989). Sarcomere lengths in the arm muscles of *H. mira* are generally <850 nm long, which is less than those measured throughout the trunk (1.087–1.351 µm long). Importantly, our quantitative measurements on arm and trunk muscles are incomplete because of the difficulty in sectioning circuitous muscles from their origins to insertions. And while confocal observations might aid in these measurements (z-lines can be observed along a muscles length; see Fig. 6a), the resolution is not high enough for precise measurements.

Still, these differences in sarcomere lengths are somewhat comparable to the conditions measured in the "fast" and "slow" muscles of planktonic, microscopic arthropods that engage in rapid movements. For example, the thoracic muscles of a cypris larva (generally under 200 µm long) that function in appendage locomotion have average sarcomere lengths of 1.7 µm, which is less than one-third the length of the sarcomeres in "slow" muscles that contribute to postural movements (Lagersson 2002). Similar quantitative differences between fast and slow muscles have been noted for a variety of other aquatic crustaceans (Medler and Mykles 2015).

Lastly, we note that *H. mira* shares many other characteristics with microscopic, aquatic arthropods of similar size and swimming styles, e.g., cypris larvae of barnacles (Lagersson 2002) and nauplius larvae of other aquatic crustaceans (Borg et al. 2012). These microfauna tend to have cross-striated muscles that supply highly setose appendages. However, unlike crustaceans, the setae of *H. mira* are not innervated and appear unlikely to have sensory functions (e.g., see Paffenhöfer and Loyd (2000) and Yen et al. (2015) for details on copepod setae). Still, the setae are likely to be important for propulsion at low Reynolds numbers as they are for copepods (Cheer 1987). Copepod nauplii have three pairs of setose appendages that engage in metachronal beat patterns and result in rapid forward jumps with erratic translation followed by backward "inefficient" locomotion (Borg et al. 2012). The power strokes create forward propulsion when the appendages and setae fan out to maximize surface area, while the recovery strokes produce backward propulsion even though the appendages and setae have collapsed rearward to minimize surface area (Borg et al. 2012). High-speed video analysis of *H. mira* has yet to reveal how the arms and setae function during the rotifer's jumps, but we hypothesize that they might function in a similar way (maximizing surface area in power strokes), albeit with different results. The rotifer's arms are arranged radially around the body, and a power stroke would translate into the arms being abducted (from resting position) rather than adducted as in crustaceans. A quick abduction would propel the rotifer backward, unless different arms take up different resting positions, which might explain why these rotifers appear to "tumble" through the water during evasion (Hochberg and Ablak Gurbuz 2008). Also, as shown in the current study, some of the setae might form joints with the arms, which if proven true (perhaps verifiable with scanning electron microscopy), would indicate their ability to collapse during recovery strokes.

Based on our data, and those in the literature (Gilbert 1985, 1987; Kirk and Gilbert 1998), we conclude that species of *Hexarthra* and *Polyarthra* might be the soft-bodied analogues of crustacean larvae, though with the added dimension of possessing locomotory cilia. Appendage-based locomotion in rotifers is rare, and so future observations of these unique rotifers that combine the knowledge of ultrastructure with quantitative measurements of locomotion might provide important insights into the functional morphology of rapid locomotion at low Reynolds numbers that is currently focused on microscopic crustaceans (e.g., Cheer 1987; Koehl 2001).

Acknowledgements We acknowledge the staff at the Core Electron Microscope Facility (UMM) for their assistance in the use of their TEM. NSF DEB Grant 1257110 to RH provided funding. Any opinions, findings, and conclusions or recommendations expressed in this material are those of the authors and do not necessarily reflect the views of the National Science Foundation.

References

Allen AA (1968) Morphology of the planktonic rotifer *Polyarthra vulgaris*. Trans Am Microsc Soc 87:60–69

Amsellem J, Clément P (1977) Correlations between ultrastructural features and contraction rates in rotiferan muscle. I. Preliminary observations on longitudinal retractor muscles in *Trichocerca rattus*. Cell Tiss Res 181:81–90

Amsellem J, Clément P (1988) Ultrastructure of the muscle of the rotifer *Trichocerca rattus*. II. The central retractors. Tissue Cell 20:89–108

Borg CMA, Bruno E, Kiørboe T (2012) The kinetics of swimming and relocation jumps in copepod nauplii. PLoS ONE 7(10):e47486

Brantley RK, Marchaterre MA, Bass AH (1993) Androgen effects on vocal muscle structure in a teleost fish with inter- and intrasexual dimorphism. J Morphol 216:305–318

Cheer AYL (1987) Paddles and rakes: fluid flow through bristled appendages of small organisms. J Theor Biol 129:17–39

Clément P (1987) Movements in rotifers: correlations of ultrastructure and behavior. Hydrobiologia 147:339–359

Clément P, Amsellem J (1989) The skeletal muscles of rotifers and their innervation. Hydrobiologia 186(187):255–278

Clément P, Villeneve J (1971) Membrane et reticulum sarcoplasmique dans les muscles des Rotiferes. J Micro 11:40 **(abstract)**

Clément P, Wurdak E (1991) Rotifera. In: Harrison FW, Ruppert EE (eds) Microscopic anatomy of invertebrates, volume 4, Aschelminthes. Wiley-Liss Inc, New York, pp 219–297

Epstein HF, Miller DM III, Otiz I, Berliner GC (1985) Myosin and paramyosin are organized about a newly identified core structure. J Cell Biol 100:904–915

Felix A, Stevens ME, Wallace RL (1995) Unpalatibility of a colonial rotifer, *Sinantherina socialis*, to small zooplanktivorous fishes. Invertebr Biol 114:139–144

Fernández B, Suárez L, Perez-Batista MA, Azcoitia I, Bodega G (1986) Annulate lamellae and whorl bodies in the diffuse supraoptic nucleus of the hamster. Acta Anat 126:230–236

Gilbert JJ (1985) Escape response of the rotifer *Polyarthra*: a high-speed cinematographic analysis. Oecologia 66:322–331

Gilbert JJ (1987) The *Polyarthra* escape from response: defense against interference from *Daphnia*. Hydobiologia 147:235–238

Gilbert JJ, Kirk KL (1988) Escape response of the rotifer *Keratella*: description, stimulation, fluid dynamics, and ecological significance. Limnol Oceanogr 33:1440–1450

Hochberg R, Ablak Gurbuz O (2007) Functional morphology of somatic muscles and anterolateral setae in *Filinia novaezealandiae* Shiel and Sanoamuang, 1993 (Rotifera). Zool Anz 246:11–22

Hochberg R, Ablak Gurbuz O (2008) Comparative morphology of the somatic musculature in species of *Hexarthra* and *Polyarthra* (Rotifera, Monogononta): its function in appendage movement and escape behavior. Zool Anz 247:233–248

Hooper SL, Hobbs KH, Thuma JB (2008) Invertebrate muscles: thin and thick filament structure; molecular basis of contraction and its regulation, catch and asynchronous muscle. Prog Neurobio 86:72–127

Irving T, Wu Y, Bekyarova T, Farman GP, Fukuda N, Granzier H (2011) Thick-filament strain and interfilament spacing in passive muscle: effect of titin-based passive tension. Biophys J 100:1499–1508

Josephson RK, Young D (1987) Fiber ultrastructure and contraction kinetics in insect fast muscles. Am Zool 27:991–1000

Josephson RK, Malamud JG, Stokes DR (2000) Asynchronous muscle: a primer. J Exp Biol 203:2713–2722

Kak A, Rao TR (1998) Does evasive behavior of *Hexarthra* influence its competition with cladocerans? Hydrobiologia 387(388):409–419

Kéver L, Boyle KS, Draičević B, Dulčić J, Permentier E (2014) A superfast muscle in the complex sonic apparatus of *Ophiodion rochei* (Ophidiifermes): histological and physiological approaches. J Exp Biol 217:3432–3440

Kirk KL, Gilbert JJ (1998) Escape behavior of *Polyarthra* in response to artificial flow. Bull Mar Sci 43(3):551–560

Koehl M (2001) Transitions in function at low Reynolds number: hair-bearing animal appendages. Math Methods Appl Sci 24:1523–1532

Koehler JK (1966) Some comparative fine structure relationships of the rotifer integument. J Exp Zool 161:231–243

Lagersson NC (2002) The ultrastructure of two types of muscle fibre cells in the cyprid of *Balanus amphritite* (Crustacea: Cirripedia). J Mar Biol Assoc UK 82:573–578

Levine RJC, Kensler RW, Reedy MC, Hofmann W, King HA (1983) Structure and paramyosin content of tarantula thick filaments. J Cell Biol 97:186–195

Medler S, Mykles DL (2015) Muscle structure, fiber types, and physiology. In: Chang ES, Thiel M (eds) The natural history of the crustacea, vol 4, physiology. Oxford University Press, New York, pp 103–133

Paffenhöfer GA, Loyd PA (2000) Ultrastructure of cephalic appendage setae of marine planktonic copepods. Mar Ecol Prog Ser 203:171–180

Rakus D, Gizak A, Deshmukh A, Wísniewski JR (2015) Absolute quantitative profiling of the key metabolic pathways of slow and fast skeletal muscle. J Proteome Res 14:1400–1411

Reedy MK (1968) Ultrastructure of insect flight muscle. I. Screw sense and structural grouping in the rigor cross-bridge lattice. J Mol Biol 31:155–176

Royuela M, Fraile B, Arenas MU, Paniagua R (2000) Characterization of several invertebrate muscle cell types: a comparison with vertebrate muscles. Microsc Res Tech 48:107–115

Šanto N, Fontaneto D, Fascio U, Melone G, Caprioli M (2005) External morphology and muscle arrangement of *Brachionus urceolaris*, *Floscularia ringens*, *Hexarthra mira* and *Notommata glyphura* (Rotifera, Monogononta). Hydrobiologia 546:223–229

Santos-Medrano GE, Rico-Martinez R, Velázquez-Rojas CA (2001) Swimming speed and Reynolds numbers of eleven freshwater rotifer species. Hydrobiologia 446(447):35–38

Schramm U (1978) Studies of the ultrastructure of the integument of the rotifer *Habrotrocha rosa* Donner (Aschelminthes). Cell Tissue Res 189:167–177

Segers H (2009) Annotated checklist of the rotifers (Phylum Rotifera), with notes on nomenclature, taxonomy and distribution. Zootaxa 1564:1–104

Storch V, Welsch U (1969) Über den Aufbau des Rotatorien tegumentes. Z Zellforsch 95:405–414

Vogel S (1996) Life in moving fluids. The physical biology of flow, 2nd edn. Princeton University Press, Princeton

Vye MV (1976) The ultrastructure of striated muscle. Ann Clin Lab Sci 6(2):142–151

Wallace RL, Colburn RA (1989) Phylogenetic relations within Phylum Rotifera: orders and genus *Notholca*. Hydrobiologia 186(187):311–318

Wallace RL, Snell TW, Smith HA (2015) Phylum Rotifera. In: Thorp J, Rogers DC (eds) Ecology and general biology: thorp and covich's freshwater invertebrates. Academic Press, New York, pp 225–271

Williamson CE (1983) Invertebrate predation on planktonic rotifers. Hydrobiologia 104:385–396

Williamson CE (1987) Predator-prey interactions between omnivorous diaptomid copepods and rotifers: the role of prey morphology and behavior. Limnol Oceanogr 32:167–177

Xu KY, Becker LC (1998) Ultrastructural localization of glycolytic enzymes on sarcoplasmic reticulum vesicles. J Histochem Cytochem 46:419–427

Xu KY, Zweier JL, Becker LC (1995) Functional coupling between glycolysis and sarcoplasmic reticulum Ca^{2+} transport. Circ Res 77:88–97

Yen J, Murphy SW, Fan L, Webster DR (2015) Sensory-motor systems of copepods involved in their escape from suction feeding. Int Comp Biol. doi:10.1093/icb/icv051